Experimental Study and CFD Simulation of Two-Phase Flow around Square-Section Obstacle in Enlarging Channel

Riyadh S. Al-Turaihi

College of Engineering, Dept. of Mech. Eng., Babylon University

(drriyadhalturaihi@yahoo.com)

***Abstract*-**The purpose of this paper is to study the two-phase flow around 2d body in enlargement channel. Experimental studies have been conducted in a channel with air-water flow for different air and water discharges. The experiments have been aimed to visualize the two phase flow phenomena as well as to studies effect of pressure difference through channel with square-section cylinder for different water discharges (20, 25, 35 and 45 l/min) and different air discharges (10, 20, 30 and 40 l/min). This paper concerns the model of a bubble population in the frame of an ensemble averaged two-phase flow formulation. The ability of the moment density approach to represent bubble population size distribution within a multidimensional CFD code based on the two-fluid model is studied. The results showed that the when air or water discharge increases, the mean pressure difference increases. Also, in a water slug, bubbles move slower than the liquid..

Keywords- *steady and unsteady turbulent flow, two-phase flow, enlargement.*

I. INTRODUCTION (HEADING 1)

The simultaneous flow of two different species inside a channel such as solid-liquid, liquid-liquid, gas-liquid under adiabatic/diabatic conditions with applications in the transport of oil, slurry, sedimentation etc. or that of the same species such as vapor-liquid under diabatic conditions in viz., boilers, condensers, distillation columns, desalination plants, refrigeration and air conditioning processes are common. When gas and liquid flow together in a channel the interface between the phases may take a variety of different patterns, the most complex being probably slug flow. The primary characteristic of slug flow is its inherent intermittence. An observer looking at a fixed position along the axis would see the passage of a sequence of slugs of liquid containing dispersed bubbles, each looking somewhat like a length of bubbly channel flow, alternating with sections of separated flow within long bubbles. These two states follow in a random-like manner, inducing pressure, velocity and phase fraction fluctuations (Jean 2002).

Seyoung et al. 2007 focused on the development of numerical code to deal with incompressible two phase flow around 2D hydrofoil combined with cavitation model with k-ε turbulent model. The simulation results were compared to experimental data to verify the validity of the developed code. Also, the comparison of the calculation results was made with LES results to evaluate the capability of conventional turbulence models such as k-ε model. The calculation results showed very good agreement with experimental observations even though this code could not grasp the small scaled bubbles in the calculation whereas LES can hold the real physics. Also, the calculation of cavitation in cryogenic fluid was done by implementing the temperature sensitivity in government equations. Even though the results showed good agreement with previous calculation results, further research will be needed to account for real physics of the formation of cavitation in cryogenic fluid due to temperature sensitivity. This code would be further extended to 3D compressible two phase flow for the study on the fluid dynamics around inducers and impellers in turbo pump system. Matevzˇ et al. 2008 studied the influence of the inlet boundary condition on simulation results. Experimental measurements and simulations of the flow over a hydrofoil in a closed circuit cavitation tunnel were performed. Using the LDA method the velocity profile, 365 mm upstream of the hydrofoil, was measured. PIV method combined with the LIF technique was used for the determination of the velocity field in the vicinity of the hydrofoil. Static pressure at 38 positions on the surface of the hydrofoil was measured. The CFD code Fluent was used for the simulations. A RANS approach with the k–□ RNG turbulence model was applied. Two simulations of the fluid flow were performed – one with a uniform (ideal) velocity profile at the inlet of the computational domain and the other with the experimentally determined velocity profile. The simulation with the ideal boundary condition produced rather poor results with a considerable discrepancy to the experimental measurements. On the other hand the simulation produced more accurate results when the real (measured) boundary condition was used. The influence of the boundary condition could be seen in x- and y-velocity component in the vicinity of the hydrofoil, in cp distribution on the surface of the hydrofoil and in the evolution of the velocity profiles downstream of the inlet. It was concluded that it is essential to either use the real (measured) velocity profiles for the inlet boundary condition or to assure that the real upstream flow is almost ideally uniform, if an accurate simulation result is required. Degawa and Uchiyama 2008 simulated the air–water bubbly flow around two tandem square-section cylinders with

the vortex method proposed by the authors in a prior study. The flow was experimentally investigated by Shakouchi et al 2001. The side length of cylinder (s) was 30 mm, and the distance between the cylinders was 2 s. The water Reynolds number was 10 000, and the air volumetric flow ratio to whole fluid was 0.03. Pair of Karman vortices appeared behind the first cylinder. The strength of the Karman vortex downstream of the second cylinder was larger than that for the single-cylinder. The strength of the Karman vortex reduced due to the bubble entrainment. The pressure reduction on the rear surface of the first cylinder was relaxed when compared with that on the single-cylinder. Therefore, this simulation could predict the reduction of the drag force acting on the first cylinder, which was clarified by the corresponding experimental study.

Xiangbin et al. 2008 studied supercavitation around a hydrofoil based on flow visualization and detailed velocity measurement. The main purpose of that study was to offer information for validating computational models, and to shed light on the multiphase transport processes. A high-speed video camera was used to visualize the flow structures under different cavitation numbers, and a particle image velocimetry (PIV) technique was used to measure the instantaneous velocity and vorticity fields. It was shown that the cavitation structure depends on the interaction of the water–vapor mixture and the vapor among the whole supercavitation stage. As the cavitation number was progressively lowered, three supercavitating flow regimes were observed: first, fluctuating cavity with periodic vortex shedding, then, vapor and water–vapor mixture coexist inside the cavity with a turbulent wake, and finally, a cavity largely filled with vapor and with a two-phase tail and distinct phase boundaries in the wake region. Even though the overall cavity boundary seems to be quite steady, the unsteadiness of the pressure fluctuation and mass transfer process between the vapor and the two-phase regions was substantial. Furthermore, in the cavitating region, strong momentum transfer between the higher and lower flow layers taken place, resulting in a highly even velocity distribution in the core part of the cavitating region, and the lower velocity area became smaller and, as the cavitation number lowers, moved toward the downstream. Edurne 2009 gained insight into gas-liquid intermittent flows. The chaotic distribution of turbulent interfaces between the different phases and a full understanding of their nature make the prediction of the flow characteristics and the numerical modeling of such flows a difficult and challenging task for researchers. In Edurne thesis, particular efforts were devoted to the experimental investigation of developing intermittent flows (plug and slug flows) in horizontal pipes in order to attain a thorough physical understanding of the internal structure of these two-phase flow patterns. Experimental data was acquired with specific attention to the development of stratified and wavy flow regimes to intermittent flow regimes. The distributions of the phases, several relevant flow characteristics and the behavior of the bubbles in the liquid phase were identified by means of wire-mesh sensor data. The main differences between plug and slug flow were elucidated and the influence of the slug void fraction on the characteristics of these flows as well as the behavior of the dispersed bubbles in the slug body were analyzed in detail. The simultaneous use of the Particle Image Velocimetry (PIV) technique and the Pulsed

Shadowgraph (PS) technique for the acquisition of experimental data enabled the calculation of the velocity field of the liquid phase. These techniques were adapted for horizontal two-phase pipe flows within this work, allowing the study of the kinematics of stratified, wavy, plug and slug flows. Turbulent quantities of these flows were also analyzed. Hameed et al. 2009 presented an analytical solution for local pressure drop due to obstructions in horizontal air-water two-phase flow. Various obstruction shapes with size were investigated. An analysis based on the momentum conservation through obstruction region. The relationship between two-phase multiplier and local (normalized) pressure drop with the gas superficial velocity were investigated. The results showed a higher pressure drops pointed for larger obstructions. The results were verified with experimental investigations. A correlation study on the two-phase multipliers and local pressure drop for two-phase, air water mixture flows through obstructions in horizontal channel was made, leading to the following conclusions: a) the pressure drop was strongly depended upon the obstructed blockage size, b) for two-phase flow, this generally mean that obstructions mainly intercepting the liquid phase will cause large pressure drop and c) the correlation presented could be used for valves, orifice, and sudden changes in flow cross-sections. Morten and Roger 2009 described a comparative study of lift dynamics on a hydrofoil and inlet pressure dynamics on a pump impeller vane. The hydrofoil, a rectangular planform NACA 0015 with a chord length of c=0.081m, fitted with a special arrangement that allowed the injection of gas downstream of the minimum pressure point, was tested in the St Anthony Falls Laboratory (SAFL) closed loop water tunnel at the University of Minnesota. The SAFL water tunnel is especially suited for gas injection type measurements due to high gas removal capabilities. The tests on the hydrofoil also included a full range of cavitation experiments. The pump tests were made at the Waterpower Laboratory at the Norwegian University of Science and Technology (NTNU). Upstream of the pump inlet a special bubble injection device was located. This arrangement allows a controlled amount of gas to enter the flow. The water and gas flow rates were measured separately. Lift measurements from the hydrofoil study display a striking similarity between gas loaded and cavitation lift dynamics. The pump dynamics data showed a maximum for a moderate gas void fraction. It was also observed that a more pronounced low frequency dynamics is present for the gas-loaded systems.

Since the coupling of cavitation modeling with turbulent flow is the difficulty topic, a numerical simulation for two phase flow with the enlargement and existence of a cubic cylinder remains as one of the challenging issues in the society. So, this study is concerned with the effects of wide range of air/water discharge in the steady and unsteady cases on the flow behavior with the enlargement from the circular tube of the water phases which contains the air phase tube, to the rectangular duct with the existence of a cubic obstacle.

II. THE EXPERIMENTAL APPARATUS

Fig.1 shows a schematic and photograph of the experimental Apparatus and measurements system. The rig is consists of, as shown in Fig. 2:

1- Main water tank of capacity (1 m3).

2- Water pump with specification quantity (0.08 m3/min) and head (8 m).

3- Valves and piping system (1.25 in)

4- Adjustable volume flow rate of range (10-80 l/min) is used to control the liquid (water) volume flow rates that enter test section.

5- Air compressor and it has a specification capacity of (0.5 m3) and maximum pressure of (16 bars).

6- Rotameter was used to control the gas (air) volume flow rates that enter the test section. It has a volume flow rate range of (6-50 l/min).

7- Valves and piping system (0.5 in) and gages.

8- Pressure transducer sensors which are used to record the pressure field with a range of (0-1 bar) and these pressure transducer sensors are located in honeycombs at the entrance and at the end of the test section. The pressure sensors with a distance of (80 cm) between each other are measuring with an accuracy of (0.1%).

9- The cubic box or cylinder used is made of stainless steel and its dimensions are (3×3×3 cm) which is coated with a very thin layer of black paint and its center located at (11.5 cm) from the entrance of the test section.

10- The test section is consisting of rectangular channel and a square-section box. The rectangular cross sectional area is (10 cm × 3 cm) and has length of (70 cm) which is used to show the behavior of the two phase flow around the cubic box and to measure the pressure difference and records this behavior. The cubic cylinder is mounted and fixed by screw and nut on a blind panel on the bottom of the rectangular channel. The three large Perspex windows of the channel (two lateral sides with lighting and the top side) allowing optical access through the test section. Two enlargement connecting parts are made of steel and manufactured with smooth slope. The first on is used to connect the test section with the outside water pipe in the entrance side while the second one is used to connect the test section with the outside mixture pipe in the exit side. The inside air pipe, in the entrance side, is holed and contained inside the water pipe by a steel flange.

11- Interface system consists of two parts which are the data logger and the transformer which contains in a plastic box. The data logger has a three connections two of them are connected to the outside of the box (one connected to the sensors and the other connected to the personal computer), the third connection is connected to the transformer, which is work to receive the signals as a voltage from the sensors and transmit it into the transformer and then re-received these signals after converting it to ampere signals in the transformer.

12- The interface system which is connected with a personal computer so that the measured pressure across the test section is displayed directly on the computer screen by using a suitable program.

13- A Sony digital video camera recorder of DCR-SR68E model of capacity 80 GB with lens of Carl Zeiss Vario-Tessar of 60 x optical, 2000 x digital is used to visualize the flow structure. The visualized data are analyzed by using a AVS video convertor software version 8.1. A typical sequence snapshots recorded by the camera using a recording rate of 30 f/s.

The flows of both gas and liquid are regulated respectively by the combination of valves and by-passages before they are measured by gas phase flow meter and liquid phase flow meter. The gas phase and the liquid phase are mixed in the enlargement connection part before they enter the test section. When the two-phase mixture flows out of the test section, the liquid phase and the gas phase are separated in liquid storage tank. Experiments were carried out to show the effect of different operation conditions on pressure difference across the test section and to visualize the flow around the cubic cylinder. These conditions are water discharges and air discharges. The selected experimental values for water discharges are (20, 25, 35 and 45 l/min) and for air discharges are (10, 20, 30 and 40 l/min).

The experimental procedures are:

1- Turn on the water pump at the first value (20 l/min).

2- Turn on the air compressor at the first value (10 l/min).

3- Record the pressure drop through the test section and photograph the motion of the two-phase flow by the digital camera.

4- Repeat the above steps by changing the water discharge.

5- Repeat the above steps by changing the air discharge.

These give sixteen (16) cases for volume fraction (Air/Water ratios).

III. NUMERICAL MODELLING

The computational fluid dynamics (CFD) software have been applied for the numerical simulation for adiabatic gas-liquid flow characteristics through a horizontal channel contain a cubic cylinder with smooth expansion from the liquid pipe in steady, unsteady and 2D cases. Air-water couple has been selected as the representative of the gas-liquid two-phase flow. Construction of the numerical domain and the analysis are performed via GAMBIT and FLUENT (ANSYS 13.0) CFD codes, respectively. Two-phase flow variables such as void fraction and flow velocity for liquid (water) and gas (air) at the inlet condition, and the geometrical values of the system (i.e. channel length, width and height, pipes and inlet

enlargement connecting part dimensions, and cylinder dimensions) used in the analysis are selected as the same variables as the experimental part. Atmospheric conditions are valid for the experimental facility. Total test rig length in the experiments, thus in the numerical domain, is (100 cm) including (70 cm) for the test section containing cylinder, and (30 cm) for the inlet enlargement part. Water pipe diameter is (3.175 cm) and air pipe diameter is (1.27 cm) as shown in Fig. 3.

The enlargement connecting part length consists of: (0.05 m) circular pipe, (0.15 m) diverge-link to change the shape from circular to rectangular and (0.1 m) rectangular duct. Air and water are selected to be working fluids and their fluid properties are in Table 1.

TABLE 1. PROPERTY PARAMETERS OF THE GAS AND LIQUID IN CFD.

Fluid	Density (kg/m³)	Viscosity (kg/m.s)	Surface Tension
Water	998.2	10.03×10^{-04}	0.072
Air	1.225	1.7894×10^{-05}	---

The model geometry structure was meshed by the preprocessor software of GAMBIT with the Quad/Submap grids. After meshing, the model contained 16282 grid nodes and 32090 faces for 2D before importing into the processor Fluent for calculation. This refinement grid provided a precise solution to capture the complex flow field around the square box and mixing region in the enlargement connecting part. The boundary conditions are the velocity inlet to the air and water feeding (Table 2) and the pressure outlet to the model outlet. A full geometry is considered because of the asymmetry behavior of the mixture that appeared in the movies when photographing the experiences as will be shown later. In Fluent, the Eulerian Multiphase Model was adopted to simulate the flow. The Eulerian multiphase model is a result of averaging of N_S equations over the volume including arbitrary particles + continuous phase and the result is a set of conservation equations for each phase (continuous phase + N particle "media") (FLUENT 2006). Because the flow rates of the air and water in the channel are high, the turbulent model (k-ε Standard Wall Function) has been selected for calculation. The solution methods details and other selections for steady and unsteady cases are described in Table 3. The Pressure-Velocity Coupling Scheme is Phase Coupled SIMPLE (Semi-Implicit Method for Pressure-Linked Equations) and the schiller-naumann scheme for the drag coefficient and manninen-et-al for the slip velocity. The time step (for unsteady case) and maximum number of iteration have been selected with proper values to enable convergence for solution which is about (0.001) for all parameters.

TABLE 2. AIR-WATER FLOW CASES.

Case number	Air/water discharges (l/min)	Air/water mass flow rates (kg/sec)	Case number	Air/water discharge (l/min)	Air/water mass flow rates (kg/sec)
1	10/20	0.1667/0.3333	5	20/20	0.3333/0.3333
2	10/25	0.1667/0.4167	6	20/25	0.3333/0.4167
3	10/35	0.1667/0.5833	7	20/35	0.3333/0.5833
4	10/45	0.1667/0.7500	8	20/45	0.3333/0.7500
Case number	Air/water discharge (l/min)	Air/water mass flow rates (kg/sec)	Case number	Air/water discharge (l/min)	Air/water mass flow rates (kg/sec)
9	30/20	0.5000/ 0.3333	13	40/20	0.6667/0.3333
10	30/25	0.5000/ 0.4167	14	40/25	0.6667/0.4167
11	30/35	0.5000/ 0.5833	15	40/35	0.6667/0.5833
12	30/45	0.5000/ 0.7500	16	40/45	0.6667/0.7500

TABLE 3. THE SOLUTION METHODS DETAILS AND OTHER SELECTIONS FOR FLUENT

Spatial Discretization		
Gradient: Green-Gauss Cell Based, Momentum Equation: First-order Up-wind		
Solver type	k-ε Model	Solution Methods
Pressure-Based	Cmu=0.09, C1-Epsilon=1.44, C2-Epsilon=1.92	Volume Fraction and Turbulent Kinetic Energy (First-order Up-wind)
Starting Solution Controls (Under-Relaxation Factors)		
Pressure=0.3, Momentum=0.7, Turbulent Kinetic Energy & Turbulent Dissipation Rate=0.8		
Specification Method for turbulence		
Intensity and Hydraulic Diameter (Turbulent Intensity=3% and Hydraulic Diameter=0.0127 m)		

The hydrodynamics of two-phase flow can be described by the equations for the conservation of mass and momentum, together with an additional advection equation to determine the gas-liquid interface. The two-phase flow is assumed to be incompressible since the pressure drop along the axis orientation is small. For the incompressible working fluids, the governing equations of the Eulerian Multiphase Model are as following (FLUENT 2006 & ANSYS 13):

-   The continuity equation is:

$$\frac{\partial(\alpha_q \rho_q)}{\partial t} + \nabla \cdot (\alpha_q \rho_q u_q) = \sum_{p=1}^{n} \dot{m}_{pq} \qquad (1)$$

Where α_q is the volume fraction for the qth phase:

-   The momentum equation for q^{th} phase:

$$\frac{\partial(\alpha_q\,\rho_q\,u_q)}{\partial t}+\nabla\cdot(\alpha_q\,\rho_q\,u_q\,u_q)=$$
$$-\alpha_q\nabla p+\alpha_q\,\rho_q\,g+\nabla\cdot\tau_q$$
$$+\sum_{p=1}^{n}(\Re_{pq}+\dot{m}_{pq}\,u_q)\qquad\qquad(2)$$
$$+\alpha_q\,\rho_q(F_q+F_{lift,q}+F_{vm,q})$$

Where the first left hand side term is referring to the transient and the second one is refer to the convection. In the right hand side, the terms are referring to the pressure, body force, shear stress, (interphase forces exchange and interphase mass exchange) and (external, lift, and virtual mass forces) respectively. Hence, solids pressure term is included for granular model. The inter-phase exchange forces are expressed as:

$$\Re_{pq}=K_{pq}(u_p-u_q)\qquad\qquad(3)$$

Where K_{pq} is the exchange coefficient and in general $F_{pq}=-F_{qp}$.

In FLUENT application, boundary conditions like "mass-flow-inlet" is taken as the inlet condition for water and air while "interior" and "outflow" are employed as the water-air mixture. Air is injected to the water via an air pipe in the experiments, therefore, the gas flow through the air pipe and the mixture occurred outlet of it are modeled in 3D (Fig. 3). According to the simulation, air with known mass flow rate flows through air pipe and then disperses into the water at the exit of the pipe. At air flow rates (thus volumetric void fraction), phase mass flow rate and void fraction profiles obtained at the air and water pipes outlet are extracted from the experimental calculations in order to be introduced as the inlet condition for the flow analysis regarding the numerical 2D domain. In the present study bubble diameter is equal to (1 cm). Assuming the bubbles are in spherical shape and neglecting the coalescence between them along the channel.

IV.   EXPERIMENTAL RESULTS

The experimental results are represented as visualizations of a cubic cylinder in gas-liquid flow through channel for different water discharges (20, 25, 35 and 45 l/min) and different air discharges (10, 20, 30 and 40 l/min) as photographs and pressure graphs.

A.   Effect of Water Discharge

Fig.s (4-a, b, c & d) show photographs for the two phase flow behavior around the square-section cylinder for water discharge (Qw=20 l/min) and air discharges (Qa=10, 20, 30 and 40 l/min) from top to bottom respectively. Photographs (4-a & b) describe the flow behavior and it appears that it is near to slug or plug region. This is due to the low velocity of air at low air discharge. From a fundamental point of view

slug flow belongs to the class of intermittent flows: the flow is unsteady even if the phase flow rate remains constant with time. Also when increase the air discharge the size and number of bubbles increases and the bubble cavities develops to cloud cavitations especially at high air discharge. This is due to the high velocity of air at high air discharge which leads to more turbulence in the flow and the flow becomes bubbly as shown in photographs (4-c & d). Fig.s (5-a, b, c & d) show photographs for the two phase flow behavior for water discharge (Qw=25 l/min) and air discharges (Qa=10, 20, 30 and 40 l/min) from top to bottom respectively. It is clear that the flow becomes unstable and unsymmetrical around the cubic cylinder and the number and size of bubble become higher compared with the previous case. It appears that the vortices behind and beside the cylinder becomes more strong compared with the previous case. Fig. 6 represents photographs for the flow behavior around the cylinder for water discharge (Qw=35 l/min) and the same air discharges. While Fig. 7 represents photographs for water discharge (Qw=45 l/min) and the same air discharges. More unsteady behavior is noticed and the flow oscillates between bubble and disperse regions. When air discharge increases with increase water discharge, flow becomes unsteady, vortices developed around the cubic cylinder surface and most bubbles transformed to cloudy flow, then a disperse region and strong vortex shedding is observed.

The experimental data shows that the average number of bubbles generally increases with increasing mixture velocities. Independently of the inlet velocities, the highest number of bubbles is found in the mixing region. Moreover, higher gas velocities have a higher number of bubbles in the mixing region. Also when water discharge increases, high turbulence appears which generate more bubbles and waves. This is due to the important effect of the cylinder existence in rectangular channel which effect on pressure difference across the inlet and outlet the channel.

B.   Effect of Pressure Difference

Fig. 8 represents the mean pressure difference with water discharge for different values of air discharge. When air or water discharge increases, the mean pressure difference increases. This is due to the increase of air or water discharge resulting in velocity increases. It is already noticed that the mean pressure difference has a significant influence on two-phase flow behavior. Therefore, it is expected that the flow instability will also depend upon the pressure difference.

C.   Effect of Time Evolution of Pressure

Fig. 9 represents the effect of time evolution of pressure obtained by experiments for water discharge Qw=20 l/min and air discharge Qa=10 l/min at inlet and outlet of the rectangular channel across the cubic cylinder. The pressure sensor at the inlet -after honeycombs- and outlet of the test section are record pressures that fluctuating as a function of time due to two-phase effect.

V. NUMERICAL RESULTS

The numerical results are represented as contours and vectors for the same air-water discharges cases in the experimental part (Table 2). As mentioned above, the 2D inlet (line) air or water discharges are calculated from the 3D experimental inlet (surface) area from the air or water discharge.

A. Steady State

Fig.s (10-a, b, c, d, e, f, g and h) depict volume fraction (water) contours for selected cases (case4, 5, 6, 7, 10, 14, 15 and 16 respectively). The differences between the experimental snapshots and numerical Fig.s are due to two reasons; the first is the differences in the overall flow rates of air and water for the same inlet velocities from the inlet regions (small lines in 2D numerical cases and big square and annulus areas in 3D experimental cases), and the second reason is that the snapshots are taken roughly from the experimental movies for each case and may be for another snapshot from the same case movie, the differences will be less. From Fig. 10 it is appear that a slug to disperse regions flow pattern is achieved. The flow rates of air and water have a large range and the figures show how the volume fraction affected the flow behavior. According to the figures, stratified water-air mixture enters the singularity section and begins to decelerate due to the smoothly enlarging cross-section. A uniform dispersed two-phase flow, in which the dispersed phase (either air bubbles or water droplets) moves with their carrier fluid (water or air), approaches to a square-section obstacle. Due to strong changes of both magnitude and direction of local velocities of the fluid flow (i.e. local fluid velocity gradients) and density difference between the dispersed phase and the fluid, the local phase distribution pattern changes markedly around the obstacle.

Fig.s (11-a, b, c, d, e and f) show selected focused area of velocity vectors colored by volume fraction (water) for other selected cases (2, 3, 8, 9, 11 and 13 respectively). These figures represent the calculated local velocities in the flow field around the cylinder with the potential flow region at different air/water velocity ratios. Strong air flows are induced and a strong vortex is created as a result of the entered air and small vortices are also produced. A recirculation zone in the wake, a flow separation at the edge of the obstacle and a wavy motion are noticed. Also, when air velocity increases, separation area is detected after the obstacle.

B. Unsteady State

Fig.s (12-a, b, c, d, e and f) represent volume fraction (water) contours development for randomly selected unsteady case1. It show how the volume fraction develops with time. As can be seen, there are unsteady asymmetrical pattern recirculating zones behind the cubic cylinder.

VI. CONCLUSIONS

The study has focused on phase distributions in low quality dispersed two phase flows around obstacle. It consists of a theoretical part of a more general nature and an experimental part highlighting bubbly flows around a cylinder in horizontal channel. Concluding remarks are summarized below:

1- Random-like manner, inducing pressure, velocity and phase fraction fluctuations: the flow is unsteady, even when the flow rates of gas and liquid are kept constant at the channel inlet.

2- The pressure sensor at the inlet and outlet of the test section are record pressures that fluctuating as a function of time due to two-phase effect. Also, when air or water discharge increases, the mean pressure difference increases.

3- Due to strong changes of both magnitude and direction of local discharges of the fluid flow and density difference between the dispersed phase and the fluid, the local phase distribution pattern changes markedly around the obstacle.

4- It should be noted that the prediction on the bubble size does not correctly describe the size observed in experiments. This is due to the difference in the numerical definition of vapor bubble and visual bubble boundary.

5- In a water slug, bubbles move slower than the liquid. The average velocity of the bubbles is slightly slower than the slug tail velocity. This means that the dispersed bubbles in the liquid slug will be caught up by the arriving elongated bubble.

6- In this study, diameter of the bubbles is considered constant and coalescence between the bubbles is neglected. However, bubbles in the actual flow break down and unite as the flow develops along the channel and this gives a varying diameter distribution which causes lift and drag forces to be calculated locally. Therefore, a simulation considering the effects of differing bubble diameter and interfacial forces is suggested for better modeling of the flow investigated.

REFERENCES

[1] ANSYS 13.0 Help, FLUENT Theory Guide, Mixture Multiphase Model.

[2] Edurne Carpintero Rogero, "Experimental Investigation of Developing Plug and Slug Flows", TECHNISCHE UNIVERSITÄT MÜNCHEN, thesis, 2009.

[3] Esam M. Abed and Riyadh S. Al-Turaihi, "Experimental Study of Two-Phase Flow around Hydrofoil in Open Channel", Journal for Mechanical and Materials Engineering, Iraq, 2012, accepted and submitted for publication.

[4] FABRE Jean, "Modelling and Control of Two-Phase Flow Phenomena", International Centre for Mechanical Sciences, Udine (Italy), September 9-13, 2002.

[5] Hameed Balassim Mahood, Hala A. Kadim and Ali N. Salim, "Effect of Flow-Obstruction Geometry on Pressure Drops in Horizontal Air-Water Two-Phase Flow", Al-Qadisiya Journal For Engineering Sciences, Vol. 2, No. 3, 2009, pp. 641-653.

[6] Introductory FLUENT Notes, FLUENT v6.3, Fluent User Services Center, December 2006.

[7] Matev Dular, Rudolf Bachert, Bernd Stoffel and Brane irok, "Influence of the Velocity Distribution at the Inlet Boundary on the CFD Prediction of Local Velocity and Pressure Fields around a Hydrofoil", Experimental Thermal and Fluid Science 32 (2008) 882–891.

[8] Morten Kjeldsen and Roger E. A. Arndt, "Blade Load Dynamics in Cavitating and Two Phase Flows", Proceedings of the 7th International Symposium on Cavitation, CAV2009 – Paper No. 113, August 17-22, 2009, Ann Arbor, Michigan, USA.

[9] Riyadh S. Al-Turaihi, "Experimental Investigation of Two-Phase Flow (Gas –Liquid) Around a Straight Hydrofoil in Rectangular Channel", Journal of Babylon University, Iraq, 2012, accepted and submitted for publication.

[10] Seyoung Lee, Changjin Lee, and Soohyung Park, "Unsteady Cavitation and Cryogenic Flow Cavitation around 2D Body", IEEE computer society, Fifth International Conference on Computational Science and Applications, DOI 10.1109/ICCSA.2007.49. pp. 306-312.

[11] Shakouchi, T., Tian, D., and Ida, T., "Behavior of Wake flow Behind Obstacle in a Gas–Liquid Vertical Two-Phase flow (Effects of Blockage Ratio)", (in Japanese). Trans. JSME, B, 2001, 67 (654), pp. 377–383.

[12] T Degawa and T Uchiyama, "Numerical Simulation of Bubbly Flow Around Two Tandem Square-Section Cylinders by Vortex Method", J. Mechanical Engineering Science, Proc. IMechE Vol. 222 Part C, 2008, pp. 225-234.

[13] Xiangbin Li, Guoyu Wang, Mindi Zhang and Wei Shyy, "Structures of Supercavitating Multiphase Flows", International Journal of Thermal Sciences 47 (2008), pp. 1263–1275].

[14] M. Young, The Technical Writer's Handbook. Mill Valley, CA: University Science, 1989.

Nomenclature

F_q	External force	(N)
g	Gravity acceleration	(m/s^2)
K_{pq}	Exchange coefficient	(-)
q	Number of phases	(-)
Q	Flow discharge	(l/min)
$\Re_{pq}$	Interphase forces exchange	(kg/m^2.s^2)
t	Time	(sec)
u_q	Velocity for the qth phase	(m/s)
$\dot{m}_{pq}$	Interphase mass exchange	(kg/m^3.s)

Greek Symbols

α_q	Volume fraction for the qth phase	(-)
ρ_q	Mixture density for the qth phase	(kg/m^3)
τ_q	Shear stress for the qth phase	(N/m^2)

Subscripts

a	Air
lift	Lift force
q	Secondary phase
vm	Virtual mass force
w	Water
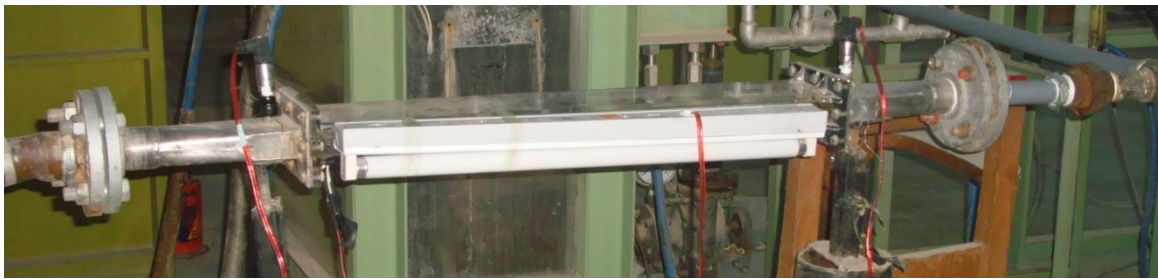
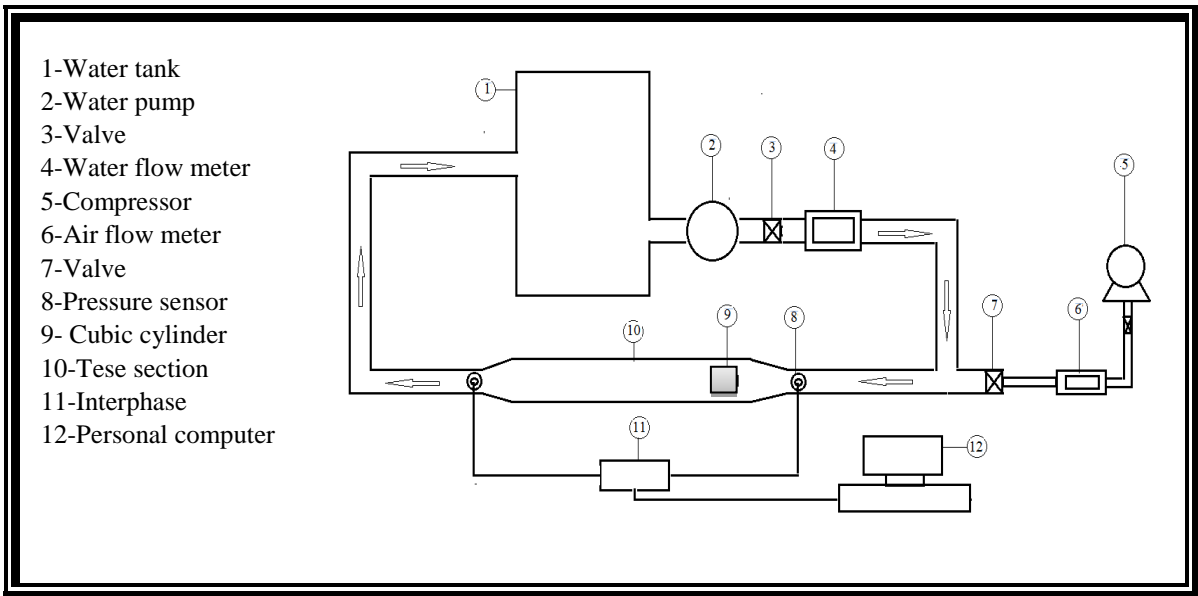Figure 1. The experimental rig and measurements system (Esam and Riyadh 2012)

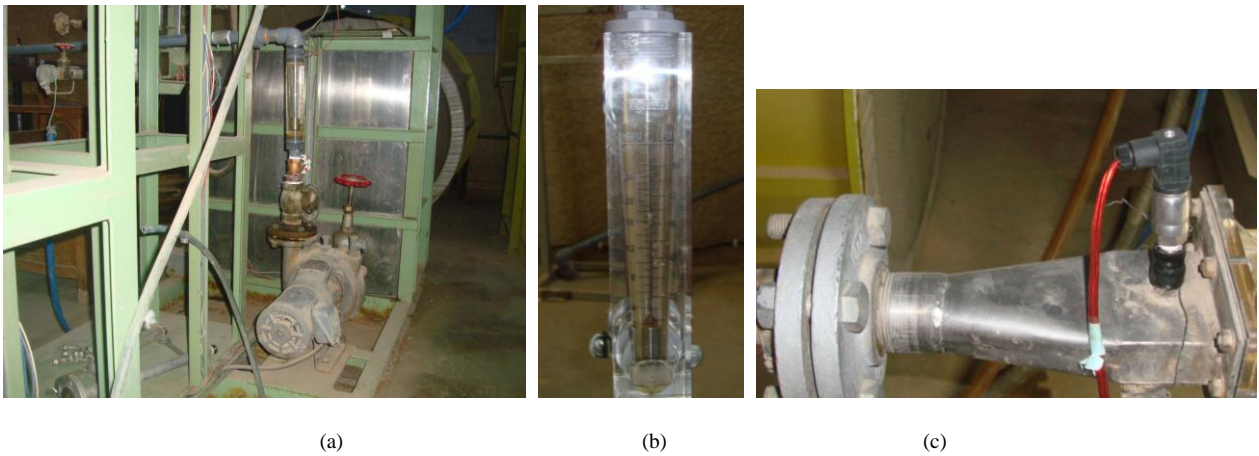(a)   (b)   (c)

Figure 2. (a) Water system, (b) Air flow meter, (c) Enlargement connecting part, flange and pressure transducer sensor (Esam and Riyadh 2012)
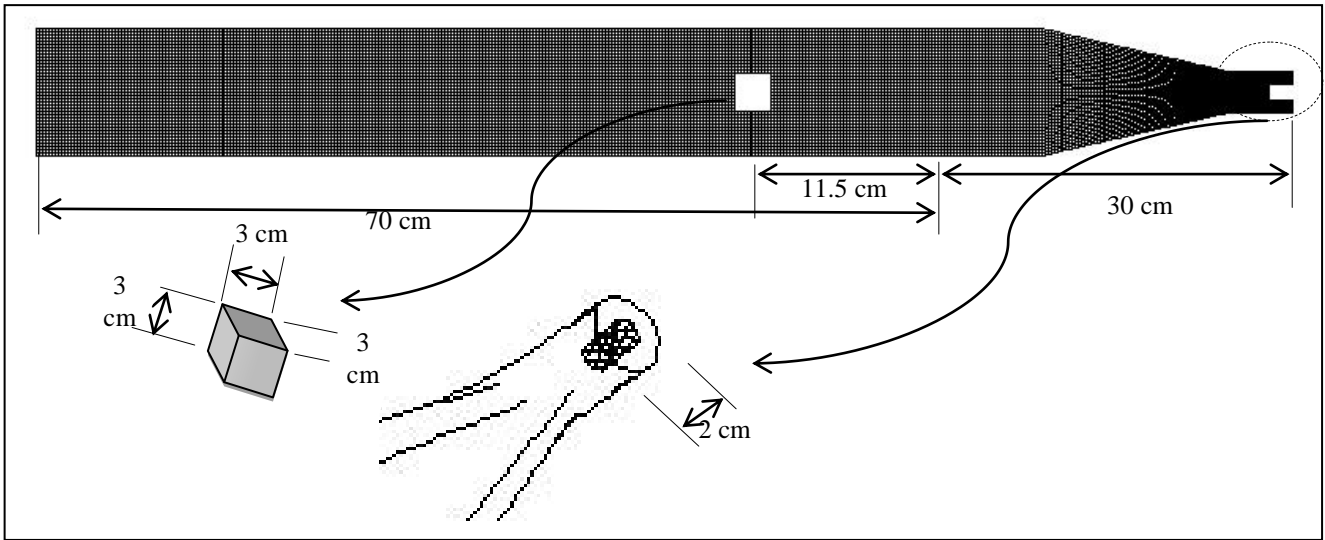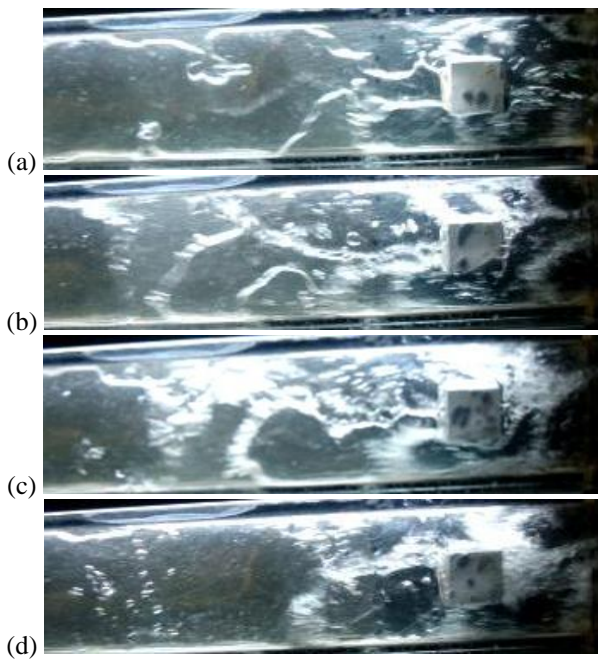
Figure 3. 2D model geometry structure mesh

Figure 4. Photographs for the two phase flow behavior for Q_a=10 l/min and Q_w=20, 25, 35 and 45 l/min respectively.
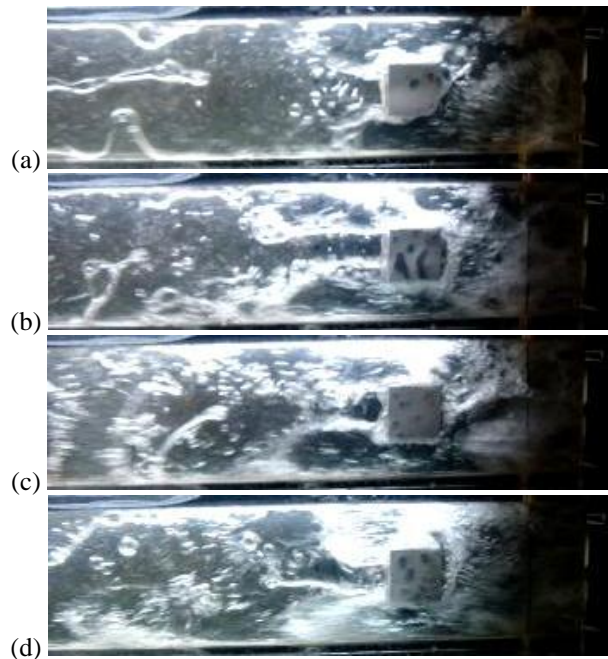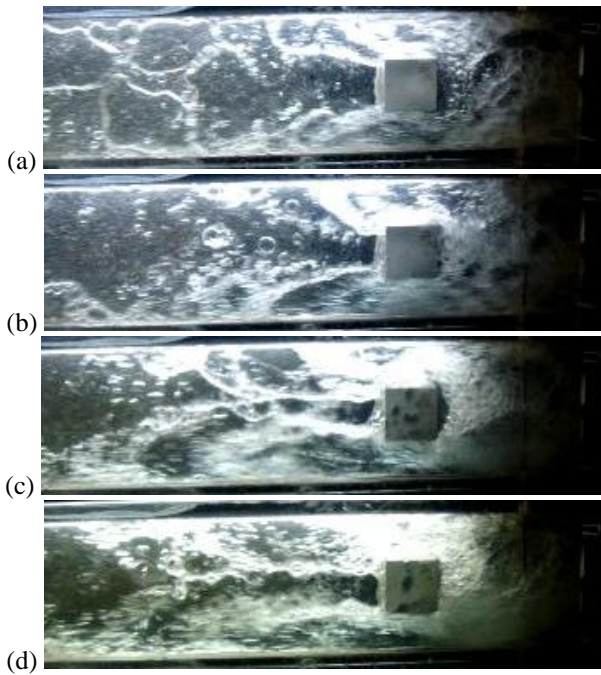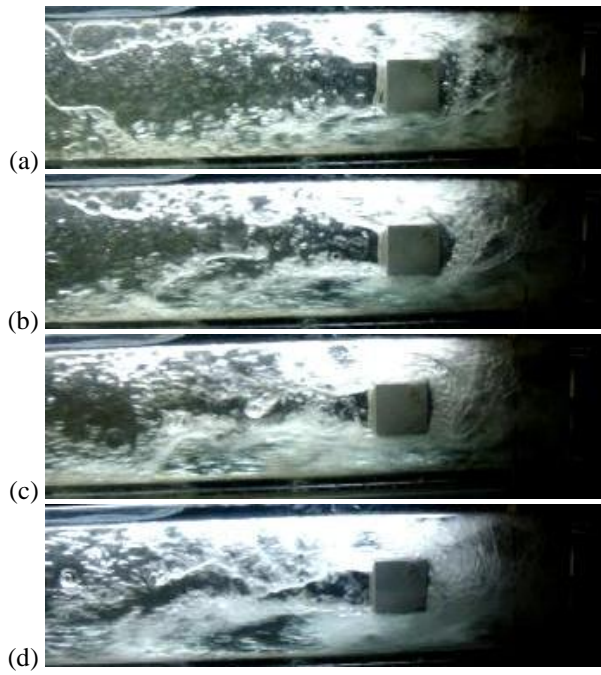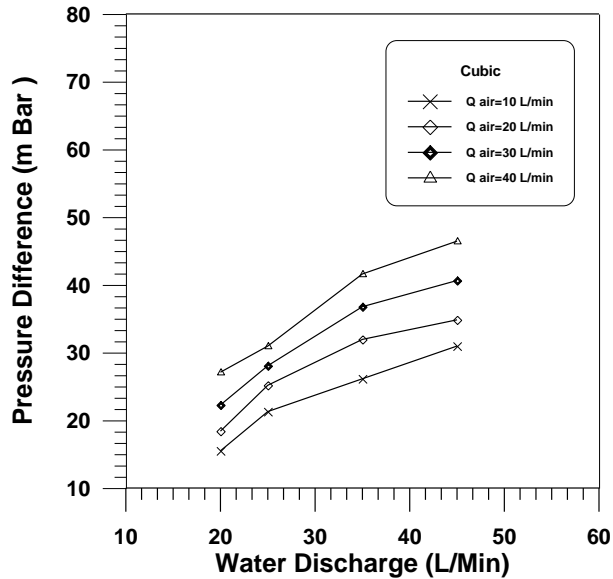

Figure 5. Photographs for the two phase flow behavior for Q_a=20 l/min and Q_w=20, 25, 35 and 45 l/min respectively.

Figure 6. Photographs for the two phase flow behavior for Q_a=30 l/min and Q_w=20, 25, 35 and 45 l/min respectively

Figure 7. Photographs for the two phase flow behavior for Q_a=40 l/min and Q_w=20, 25, 35 and 45 l/min respectively

Figure 8. Mean pressure difference with water discharge for different values of air discharge
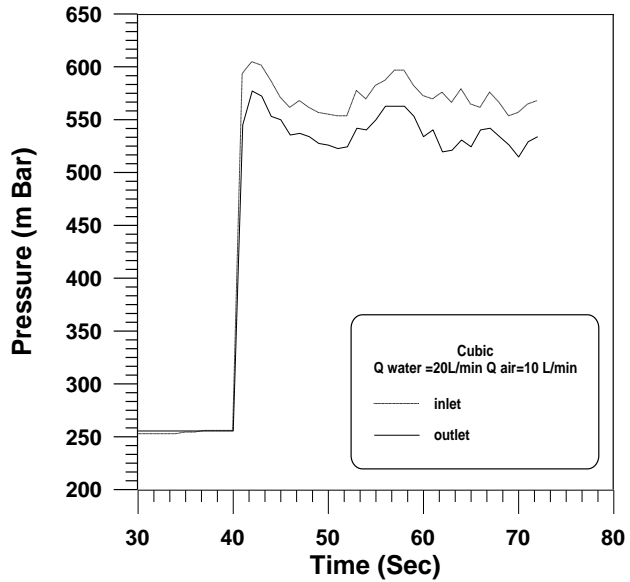
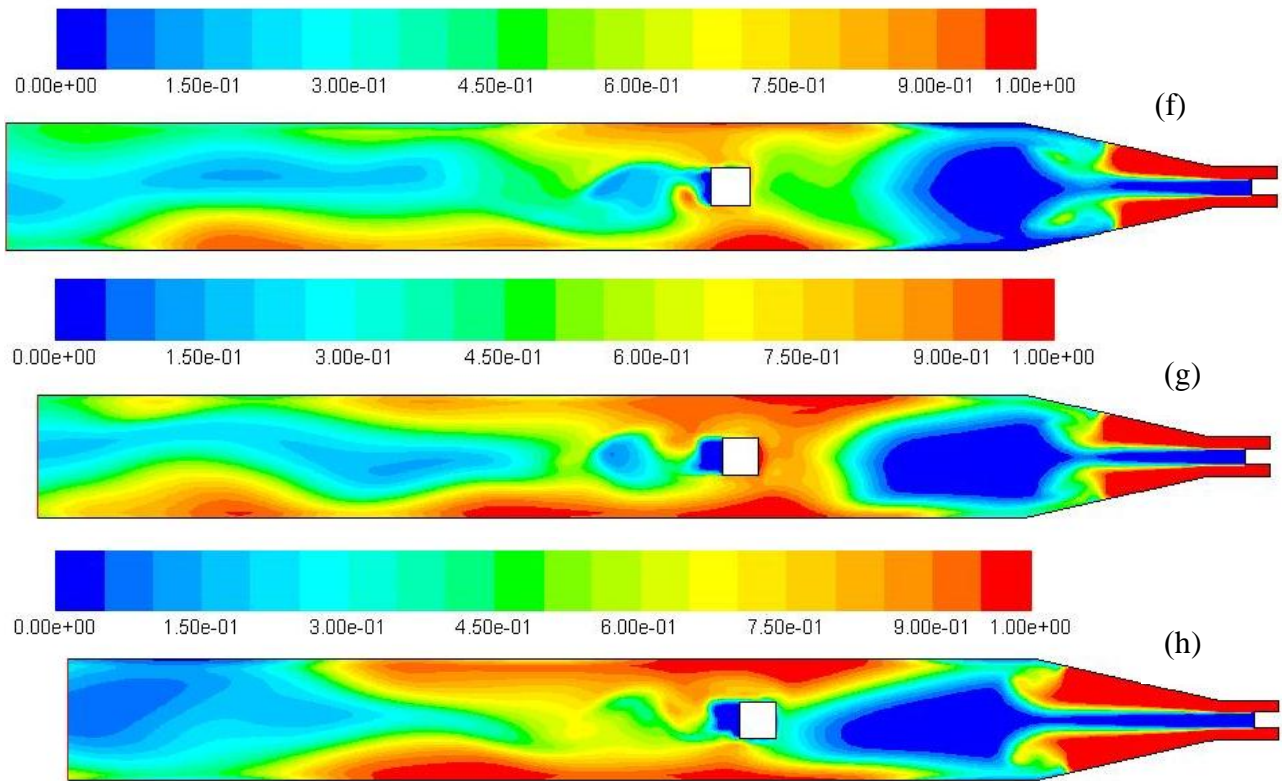Figure 9. Effect of time evolution of pressure for water discharge Q_w=20 l/min and air discharge Q_a=10 l/min.
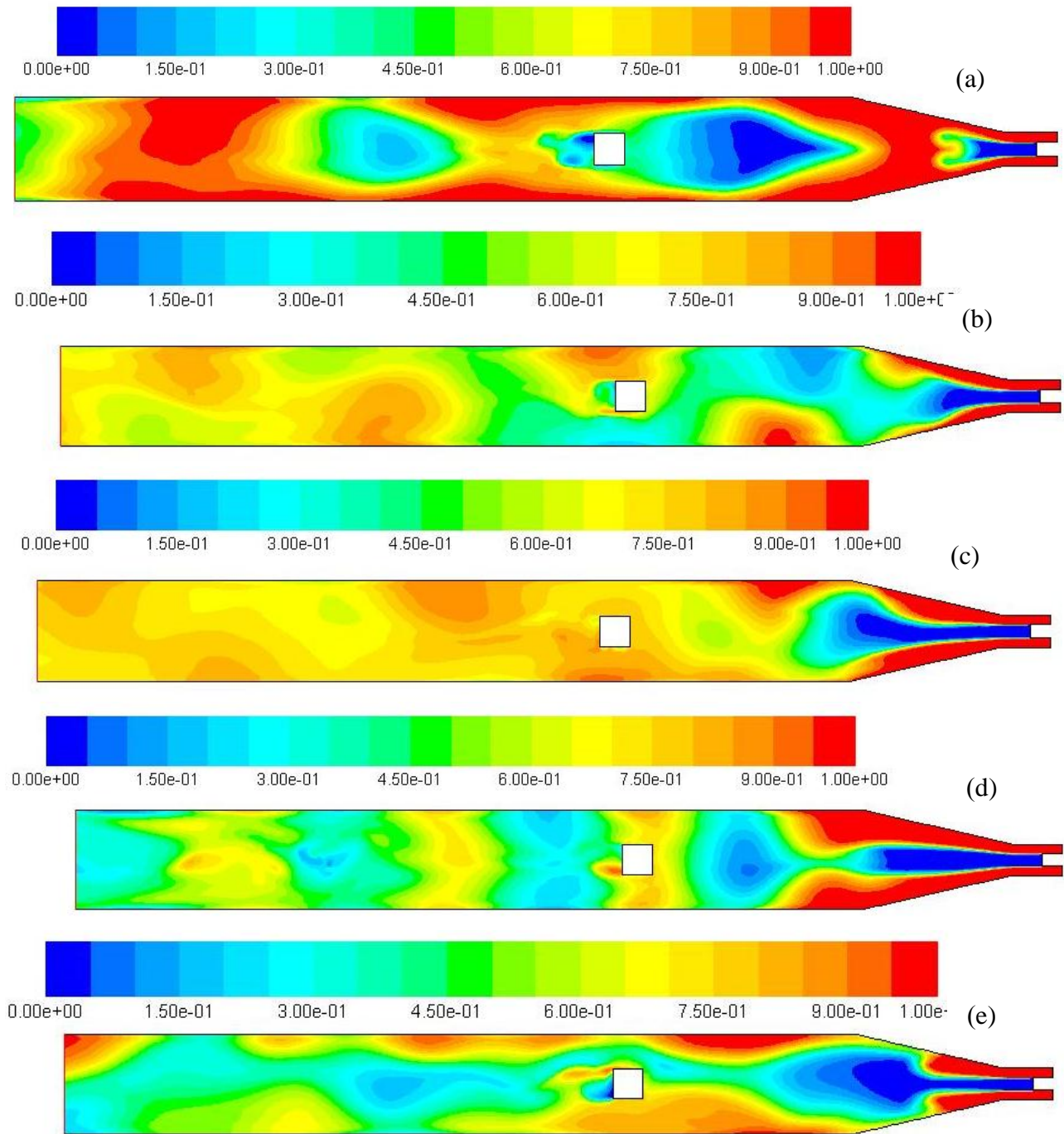
Figure 10. Volume fraction (water) contours for cases (4, 5, 6, 7, 10, 14, 15 and 16) respectively
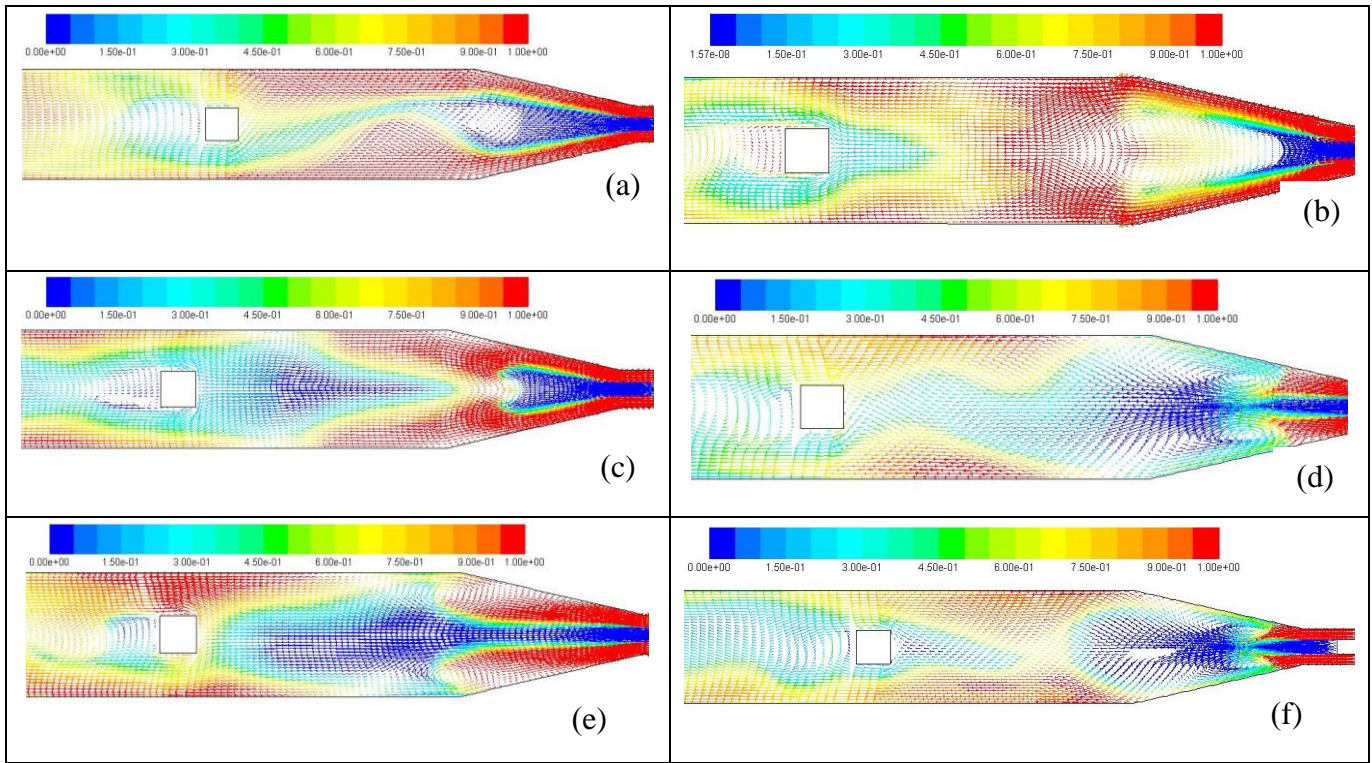
Figure 11. Velocity vectors colored by volume fraction for cases (2, 3, 8, 9, 11 and 13 respectively)
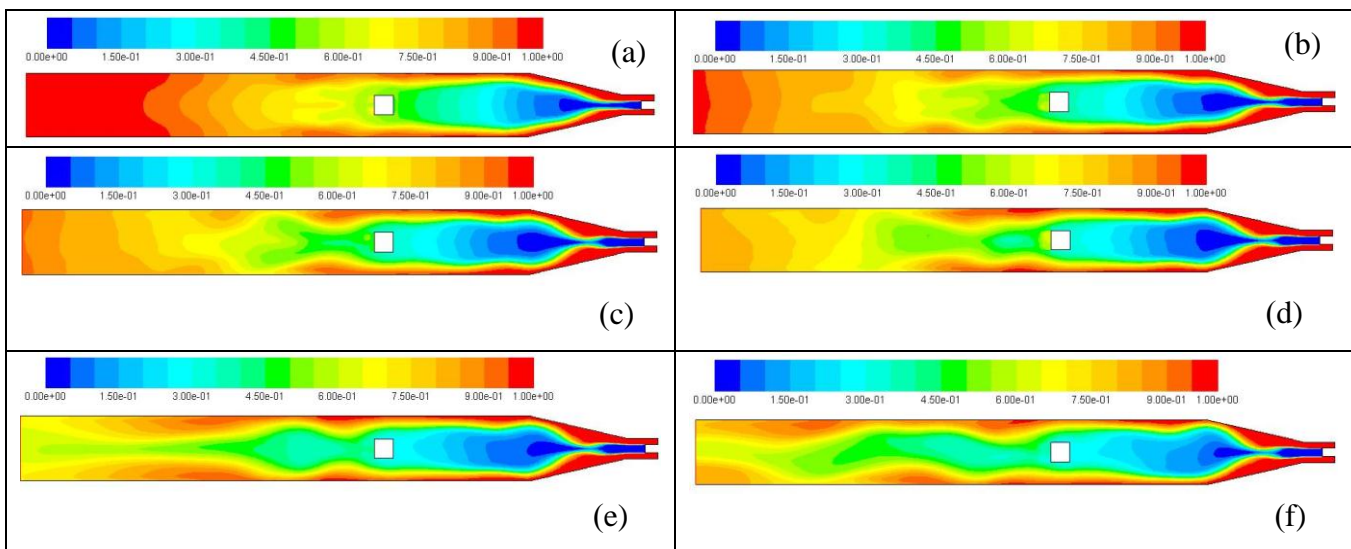
Figure 12. Volume fraction (water) contours development for unsteady case1